Size and Bandgap Control in the Solution-Phase Synthesis of Near-Infrared-Emitting Germanium Nanocrystals

Daniel A. Ruddy, Justin C. Johnson, E. Ryan Smith, and Nathan R. Neale*

National Renewable Energy Laboratory, 1617 Cole Boulevard, Golden, Colorado 80401, United States

ABSTRACT We present a novel colloidal synthesis of alkyl-terminated Ge nanocrystals based on the reduction of GeI_4/GeI_2 mixtures. The size of the nanocrystals (2.3−11.3 nm) was controlled by adjusting both the Ge(IV)/Ge(II) ratio and the temperature ramp rate following reductant injection. The near-infrared absorption (1.6−0.70 eV) and corresponding band-edge emission demonstrate the highly tunable quantum confinement effects in Ge nanocrystals prepared using this mixed-valence precursor method. A mechanism is proposed for the observed size control, which relies upon the difference in reduction temperatures for Ge(II) *versus* Ge(IV).

KEYWORDS: germanium nanocrystal · quantum confinement · bandgap control · size control · mechanism · infrared emission

Group IV nanocrystals (NCs) are a potentially nontoxic class of photoluminescent nanomaterials with applications in solar photoconversion and related optoelectronic technologies (*e.g.*, photodetectors, LEDs, biological imaging).[1,2] Despite the great potential of these materials, size- and shape-control is not nearly as well-developed for group IV nanoparticles as that for binary II−VI, IV−VI, and III−V semiconductors. Fine-tuning of NC size and shape would facilitate advances in the study of the photophysical properties (*i.e.*, absorbance and photoluminescence (PL)) associated with group IV NCs. In particular, development of synthetic protocols to reliably control sizes in the 2−10 nm range is necessary to understand their quantum confinement behavior and evaluate their efficacy in potential device structures.

Although Si and Ge are both of interest for use in optoelectronics applications, Ge is particularly attractive due to (i) a narrow bulk bandgap (0.67 eV at 300 K) that is easily tuned *via* quantization to technologically important wavelengths, (ii) a large exciton Bohr radius (~24 nm), which provides a strong quantum confinement effect,[3−5] (iii) potential behavior as a direct or quasidirect bandgap material on the nanoscale, and (iv) a large absorption coefficient ($\sim 2 \times 10^5$ cm^{-1} at 2 eV).[6] Of the strategies for preparing nanomaterials, colloidal synthesis of high-quality Ge NCs is a desirable route that would enable low-cost fabrication, processing, and device assembly.[7−10] Over the past decade a number of publications have appeared detailing solution-phase synthetic routes to Ge NCs, including (i) reduction of GeX_4 salts (X = Cl, Br, I) using Zintl complexes,[11,12] sodium,[13,14] sodium naphthalenide,[15,16] or metal hydrides;[17−19] (ii) thermolytic reduction of organogermanes[20] or $Ge[N(SiMe_3)_2]_2$ (Me = methyl);[21,22] and (iii) reduction of GeI_2 with hydrides[23] or butyllithium (BuLi).[24] In addition to colloidal approaches, reports on the preparation of Ge NCs using physical deposition methods have yielded both oxide matrix-bound[25−34] and matrix-free particles.[35,36]

Despite the extent of these synthetic efforts, significant inconsistencies exist in the photophysical properties attributed to these nanoscale semiconductors. For instance, even though the absorption properties of Ge NCs have been demonstrated by experiments[25,34] and theory[37,38] to show strong quantum size effects, early reports found that emission was relatively insensitive to particle size. The PL emission of Ge NCs prepared by physical deposition techniques was initially reported to be centered from 2.1−2.4 eV for particles having diameters from 2−15 nm,[26−30] which would be inconsistent with emission from carrier confinement in quantum dots, as a larger PL energy range would be expected. Later, the high energy PL (>2.0 eV) previously attributed to Ge NC emission was instead found to result from surface oxide impurities.[31−33]

*Address correspondence to Nathan.Neale@nrel.gov.

Received for review October 12, 2010 and accepted November 12, 2010.

Published online November 23, 2010.
10.1021/nn102728u

The latter of these papers[33] demonstrated the first example of near-infrared (NIR) emission by Ge NCs, exhibiting PL peaks of 0.88−1.54 eV (1400−800 nm) for 5.3−0.9 nm diameter particles, which is more consistent with quantum confinement from the 0.69 eV band-edge emission observed for bulk germanium.[39] Furthermore, in all but one case,[24] Ge nanoparticles prepared *via* solution-phase colloidal routes have exhibited (when reported) emission in the near-UV to blue-visible, from 340−500 nm (3.6−2.5 eV). Similar to the physical deposition literature, the near-UV to blue-visible emission in Ge NCs prepared by solution-phase routes has been attributed to uncontrolled amounts of luminescent GeO_x impurities.[24]

Of the known colloidal methods, two significant advancements in the solution-phase synthesis of Ge NCs—both based on high temperature reduction of GeI_2—were recently reported.[23,24,40] Korgel and co-workers showed that Ge NC size may be tuned from 3−11 nm by adjusting the GeI_2 concentration.[23] However, no characterization of the nanoparticle photophysics was performed. In the more recent communication, Klimov and co-workers confirmed that Ge precursor concentration does have some effect on particle size, but good size control was still lacking.[24] More importantly, this work demonstrated the first NIR emission from colloidally synthesized Ge NCs with PL peaks ranging from 980−1140 nm (1.26−1.09 eV) for 3.2−4.0 nm diameter particles, consistent with the lone report of NIR emission from physically deposited particles.[33] While these two recent communications on the reduction of GeI_2 represent progress toward size-control of Ge NCs, both have drawbacks from a synthetic standpoint. The GeI_2 precursor exhibits limited solubility in the long alkyl-chain solvents employed in NC syntheses (*i.e.*, trioctylphosphine (TOP) and hexadecylamine (HDA)). This necessitates long stirring times (12−24 h) or elevated temperatures to achieve the high concentrations necessary for larger particle growth, ultimately limiting the NC size range available with these methods.

Here, we report a colloidal synthesis method that offers reproducible control of Ge NC size from 2.3−11.3 nm by the reduction of GeI_4/GeI_2 mixtures at a constant Ge concentration. This strategy eliminates the need for high Ge precursor and reductant concentrations to synthesize larger particles. Instead, the NC size is controlled by the Ge(IV)/Ge(II) ratio and the temperature ramp rate following reductant injection. The photophysical properties of the Ge NCs, including bandgap and NIR emission energies, are found to increase with decreasing particle size as would be expected from strong quantum confinement. In addition, we propose a mechanism for the observed size control, which relies upon the difference in reduction temperature (and rate) for Ge(II) *versus* Ge(IV). Our data suggest that Ge NCs form *via* an initial low-temperature reduction of Ge(II), followed by controlled growth of the NCs through the slower reduction of Ge(IV) at higher temperatures.

RESULTS AND DISCUSSION

The synthetic protocol developed here employs a long alkyl-chain amine (HDA or oleylamine) as solvent and the soluble reductant BuLi, similar to that reported by Lee *et al.*[24] Our method is distinguished in that the Ge NC source is a GeI_4/GeI_2 mixture with a defined stoichiometry at a constant total Ge concentration, which is essential in controlling the final NC size. We label our samples **Ge-NC(Ge(IV)/Ge(II))**, where Ge(IV)/Ge(II) represents the respective molar percentage ratio of Ge precursors in the reaction. In a typical synthesis, the desired amount of GeI_4 and/or GeI_2 was dissolved in HDA while heating under flowing nitrogen. When the reaction temperature reached 200 °C, a solution of BuLi (1.1 equiv *vs* total iodide) in 1-octadecene (ODE) was rapidly injected, causing an immediate drop in temperature to *ca.* 150 °C. After recovery to 200 °C, the temperature was then increased to 300 °C (ramp rate ≈ 2.5 °C min^{-1} for all experiments except for **Ge-NC(100/0)$_{fast}$**, where it was 15 °C min^{-1}) and held for 1 h at 300 °C. The reaction undergoes characteristic color changes from yellow to orange to brown associated with the formation and growth of Ge NCs. Presumably, octadecyl surface groups form *via* well-known hydrogermylation between a transiently formed Ge−H surface species and octadecene.[24,41] The dark brown solid product was isolated *via* the commonly used solvent/nonsolvent precipitation technique and was stored in a glovebox. No attempts were made to focus the size regime using size-selective precipitation.

Representative TEM images of the **Ge-NC(Ge(IV)/Ge(II))** series are given in Figure 1A−E, and Table 1 summarizes the Ge(IV)/Ge(II) ratios investigated and resulting average NC diameters. Although in some cases particles appear to be nonspherical in shape (particularly in Figure 1D,E), in most cases this is due to overlaying particles. High-resolution images (Figure 1F−G) revealed that particles are quasi-spherical with low aspect ratios. In addition to the Ge(IV)/Ge(II) ratio, it was found that a slow ramp rate of ~2.5 °C min^{-1} from 200−300 °C was essential to reproducibly control the NC size. When a fast ramp rate of 15 °C min^{-1} was employed, the average NC size at a given Ge(IV)/Ge(II) value varied widely from batch to batch. The lone exception was when only GeI_4 was used as the Ge source, **Ge-NC(100/0)**. In this case, the extremes of NC size could be achieved by employing either the fast or slow temperature ramp rate. A fast ramp rate produced small 2.3 ± 0.4 diameter NCs, **Ge-NC(100/0)$_{fast}$**, and a slow ramp rate produced large 11.3 ± 2.4 nm diameter NCs, **Ge-NC(100/0)$_{slow}$**. When only GeI_2 was employed as the Ge source, **Ge-NC(0/100)**, the reduction yielded NCs with an average diameter of 3.8 ± 0.8 nm consistent with the report of Klimov and co-workers.[24] The NC diameter

could be increased to 4.7 ± 1.0 nm using a 50/50 ratio, **Ge-NC(50/50)**, and further increased to 6.6 ± 1.5 nm with a 75/25 ratio, **Ge-NC(75/25)**. This series demonstrates that the Ge−NC size can be tuned over a 9 nm range to have average diameters of 2.3, 3.8, 4.7, 6.6, and 11.3 nm using this synthetic methodology.

Further characterization of the **Ge-NC(Ge(IV)/Ge(II))** materials was carried out by high-resolution TEM (HR-TEM). In addition to the expected single crystal lattice fringes observed for the majority of particles in all **Ge-NC(Ge(IV)/Ge(II))** samples (Figure 1F), it was found that some NCs in each sample displayed polycrystallinity (*i.e.*, visible grain boundaries) and a small number displayed regions that appeared amorphous (Figure 1G). The fraction of NCs in these samples that possess polycrystalline/amorphous structure is difficult, if not impossible, to accurately estimate, although we stress that the majority of nanoparticles examined by HRTEM were single crystals. The incomplete crystallization of a small proportion of the NCs is attributed to the inherently high crystallization temperature of Ge that, similar to Si, has been identified as a major reason progress in the synthetic preparation of group IV semiconductor nanomaterials has lagged behind that of groups II−VI, IV−VI, and III−V.[14,42] X-ray diffraction patterns of the Ge NCs were broad, with overlapping (220) and (311) peaks, reflecting the expected peak broadening due to small crystallite size and, to some degree, polycrystallinity, consistent with previous reports of similarly sized NCs (Supporting Information, Figure S2).[18,22] As an additional check of material composition, energy dispersive X-ray spectra (EDS) were recorded, and characteristic Ge peaks were observed (not shown).

The photophysical properties of the **Ge-NC(Ge(IV)/Ge(II))** materials were investigated *via* UV−vis−NIR absorbance and PL spectroscopies (405 nm excitation). Simple quantum confinement effects suggest that smaller NCs should exhibit an absorption onset at higher energy than larger NCs. The **Ge-NC(Ge(IV)/Ge(II))** materials followed this trend extremely well, with an absorption onset of the small 2.3 nm NCs, **Ge-NC(100/0)$_{fast}$**, near 780 nm (1.6 eV), and that of the largest 11.3 nm NCs extending to 1800 nm (0.70 eV) (Figure 2A, Table 1). Similarly, the PL spectra for the Ge NCs demonstrated that the PL peak correlates with the effective bandgap, shifting from 860 nm (1.44 eV) for 2.3 nm NCs (bandgap 1.6 eV) to 1230 nm (1.01 eV) for 4.7 nm NCs (bandgap 1.1 eV) (Figure 2B, Table 1). The broad luminescence (fwhm = 250−425 nm) is indicative of emission from particle size ranges (±20%) within the samples. Notably, the fact that absorption energies were slightly higher (by ~0.1 eV) than emission energies indicates a Stokes-like shift that is consistent with vibrationally coupled emission from band-edge transitions. It is also important to highlight the absence of a direct, allowed exciton peak in any of the absorption spectra, suggesting that transition from an indirect to a direct or quasi-direct bandgap does not occur with these particle sizes. Our experiments also showed that the PL intensity significantly decreased for NCs having an absorption onset at or below 1.0 eV (~6 nm and larger), for which only extremely weak NIR PL (not shown) was detected, as has been observed previously.[24,33,40] Interestingly, this phenomenon of decreasing PL intensity with decreasing effective bandgap appears to be a general phenomenon for quantum-confined nanomaterials and has been attributed to nonradiative multiphonon transitions into dark trap states as well as energy transfer to ligand vibrations.[43,44]

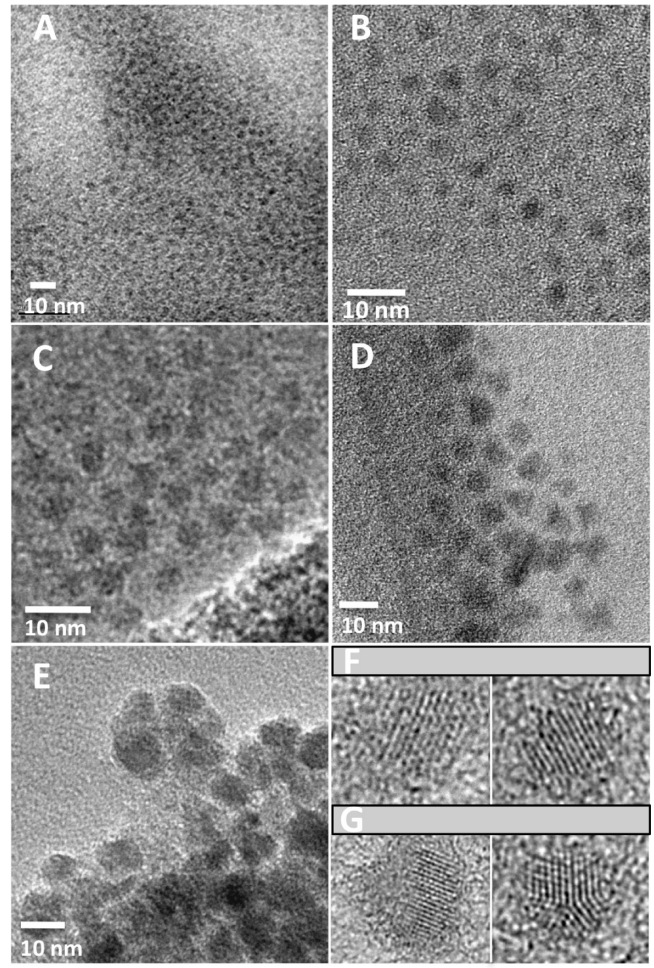

Figure 1. Representative TEM images for (A) Ge-NC(100/0)$_{fast}$, (B) Ge-NC(0/100), (C) Ge-NC(50/50), (D) Ge-NC(75/25), (E) Ge-NC(100/0)$_{slow}$, and HRTEM images showing (F) single crystal Ge NCs and (G) partially amorphous and polycrystalline Ge NCs. Lattice fringes correspond to the cubic Ge (111) reflection (*d*-spacing = 3.3 Å).

As described above, PL emission from solutions of **Ge-NC(Ge(IV)/Ge(II))** prepared under rigorously air-free conditions was observed as a broad peak in the NIR. However, after open solutions were exposed to air for extended periods of time (*i.e.*, ≥1 week), the band-edge NIR emission was completely quenched, a blue shift to visible wavelengths occurred, and a second weak visible peak was detected at 525 nm (Figure 3A). These emission changes are attributed to surface oxida-

TABLE 1. Average diameters (± 1 standard deviation) for the Ge-NC(Ge(IV)/Ge(II)) materials prepared in this study, with absorption onsets and PL peak maxima for each size[a]

Ge(IV)/Ge(II)	$100/0_{fast}$	0/100	50/50	75/25	$100/0_{slow}$
NC size (nm)	2.3 ± 0.4	3.8 ± 0.8	4.7 ± 1.0	6.6 ± 1.5	11.3 ± 2.4
absorption onset eV (nm)	1.6 (780)	1.3 (950)	1.1 (1100)	1.0 (1200)	0.70 (1800)
PL peak maximum eV (nm)	1.44 (860)	1.24 (1000)	1.01 (1230)	n/a	n/a

[a]Average diameters represent at least three independent preparations of the NCs at each Ge(IV)/Ge(II) value. Absorption onset was determined by extrapolation of the linear portion of the Tauc plots to the *x*-axis (Figure 2A). NCs with PL emission below a meaningful intensity are represented by n/a.

tion, presumably resulting from the reaction of water/oxygen with surface hydrides not passivated by octadecene. Additionally, varying the excitation wavelength from 405 (3.06) to 750 nm (1.65 eV) had virtually no effect on the PL spectrum (Figure 3B) or the PL quantum yield, in contrast to reports for colloidally grown Ge NCs exhibiting near-UV to blue-visible PL.[11,12,15,17,19,21] These data provide further evidence that, for the NCs prepared here, emission occurs from the optical bandgap, which is quantized but still in the NIR for all samples.

The PL quantum yield (QY) was determined for **Ge-NC(100/0)$_{fast}$**, **Ge-NC(50/50)**, and **Ge-NC(0/100)** (Figure 2B). The PL QY for the 6.6 nm **Ge-NC(75/25)** was also investigated, and due to the low PL intensity approaching the detection limit, it was estimated to be less than 0.01%. The PL QY values for the 2.3, 3.8, and 4.7 nm NCs were less than 0.1% in all cases, which is somewhat lower than the values of up to 8% reported previously for alkyl-passivated Ge NCs.[24] However, these values were based on the use of the reference dye IR-26; a recent study finds that the generally accepted QY of this dye has been overestimated by close to an order of magnitude,[43] which suggests that the correct QY for the Ge NCs of ref 24 is closer to 0.5−1%.[24] One potential explanation for the low QY values of the **Ge-NC(Ge(IV)/Ge(II))** materials is unpassivated surface states. For example, germanium hydrides or unsaturated germanium species (*i.e.*, Ge═Ge) may exist at the nanocrystal surface and could serve as trap states resulting in thermalized energy loss. A second possibility is the presence of HDA or other impurities (*i.e.*, trace LiI byproduct, unreduced Ge iodides). Notably, residual surfactant was occasionally observed by XRD for drop-cast NC films, and even trace amounts of amines have been shown to quench PL in Ge nanostructures.[45] Given the small proportion of polycrystalline NCs and amorphous regions (observed by TEM) in some particles, it is unlikely that this factor would contribute substantially to the low PL QY. Thus, minor impurities, along with the unpassivated surface states and vibrational energy loss processes noted previously,[43,44] are likely causes for the low PL QY values observed here. We are currently working on strategies to improve the purity, surface passivation, and crystallinity of these nanomaterials to determine the degree to which these factors affect the PL QY.

Given the successful size control achieved using this mixed-valence precursor method, it is interesting to consider the mechanism of this reaction. It is important to initially note that the Ge precursors are not expected to be solely iodides upon dissolution in stoichiometric excess of primary amines at elevated temperatures. Rather, ligand exchange would occur to produce germanium amides or amide-iodide mixed-ligand Ge complexes, as shown in eqs 1 and 2 (R = hexadecyl or oleyl).[46,47]

$$GeI_2 + x\,NH_2R \longrightarrow \underset{\textbf{[Ge(II)]}}{GeI_{(2-x)}(NHR)_x} + x\,RNH_3I \quad (1)$$

$$GeI_4 + x\,NH_2R \longrightarrow \underset{\textbf{[Ge(IV)]}}{GeI_{(4-x)}(NHR)_x} + x\,RNH_3I \quad (2)$$

$$2\,\textbf{[Ge(II)]} \rightleftharpoons Ge^0 + \textbf{[Ge(IV)]} \quad (3)$$

Additionally, it has been demonstrated that Ge crystallite nucleation occurs from the thermally activated disproportionation reaction of Ge(II) amides and iodides to

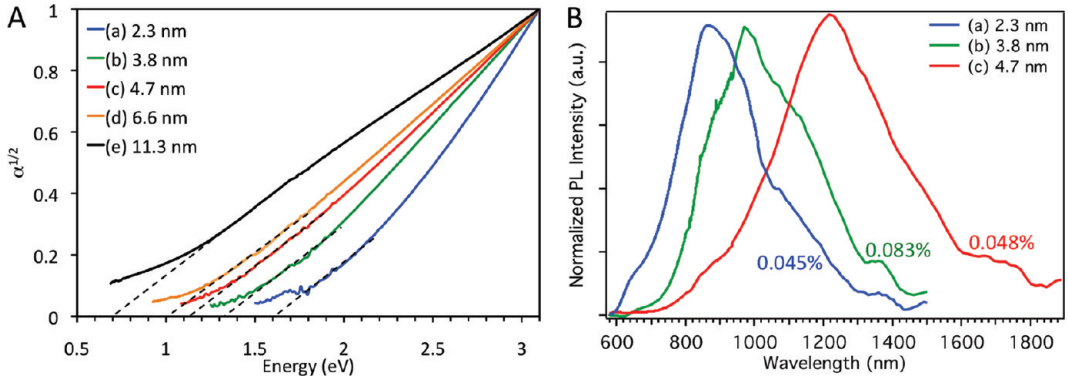

Figure 2. (A) Tauc plots of (a) Ge-NC(100/0)$_{fast}$, (b) Ge-NC(0/100), (c) Ge-NC(50/50), (d) Ge-NC(75/25), and (e) Ge-NC(100/0)$_{slow}$ calculated from the absorption data in Supporting Information, Figure S3. (B) PL spectra (405 nm excitation) of tetrachloroethylene solutions of (a) Ge-NC(100/0)$_{fast}$, (b) Ge-NC(0/100), and (c) Ge-NC(50/50). The color-coded numbers in panel B are the respective PL QY values.

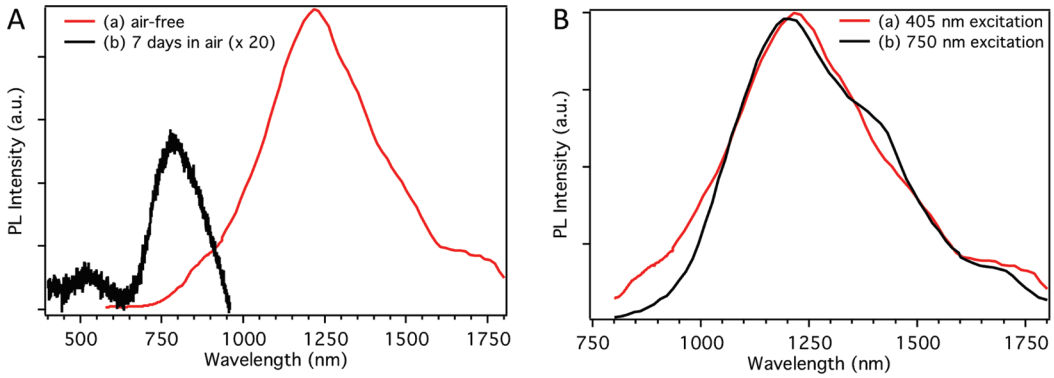

Figure 3. (A) PL emission of (a) air-free 4.7 ± 1.0 nm Ge-NC(50/50) in tetrachloroethylene (excited at 405 nm) and (b) the same sample after exposure to air for 7 days (excited at 300 nm). The intensity of the oxidized sample is increased by a factor of 20 to be on a comparable scale to the fresh sample spectrum. (B) PL emission of Ge-NC(50/50) in tetrachloroethylene as a function of excitation wavelength. QY values were found to be 0.048% with 405 nm excitation and 0.040% with 750 nm excitation.

Ge^0 and Ge(IV) at high temperature (*i.e.*, ≥300 °C) without the addition of reductant as shown in eq 3.[21,23,48] Independent experiments within the system described here verified that this disproportionation reaction occurs at even lower temperatures in HDA or oleylamine. When GeI_2 was employed as the sole Ge source (**Ge-NC(0/100)**), a characteristic color change from yellow to orange-brown occurred between 190 and 200 °C prior to reductant injection. Although the color changed to brown within minutes after the reductant was injected, attempts to isolate or image NCs from this solution—cooled to room temperature minutes after the addition of BuLi—were unsuccessful, suggesting that the brown color resulted from formation of clusters or small NC seeds (<1 nm). In contrast, reduction of solely GeI_4 (**Ge-NC(100/0)**) was observed at higher temperatures (250−260 °C) as evidenced by the same color change sequence. Notably, no color change occurred in solutions containing only **[Ge(IV)]** without addition of BuLi, demonstrating that the Ge(IV) amide−iodide complexes in eq 2 are stable up to 300 °C in the absence of a reductant. For reactions employing both GeI_2 and GeI_4, the characteristic dark brown color was observed below 220 °C, consistent with nucleation occurring from the **[Ge(II)]** precursor. The slightly higher temperature (≤220 °C) required for nucleation with solutions containing both **[Ge(IV)]** and **[Ge(II)]** *versus* the 190−200 °C required for solutions containing solely **[Ge(II)]** is attributed to the equilibrium reaction shown in eq 3, which would disfavor Ge^0 seed formation in the presence of **[Ge(IV)]**. These observations suggest that the nucleation and growth phenomena acting on Ge NC formation involve a relatively fast reduction of **[Ge(II)]** species to produce Ge^0 seeds, followed by a slower reduction of **[Ge(IV)]** complexes resulting in growth of the NCs (Scheme 1). The difference in **[Ge(IV)]** and **[Ge(II)]** concentrations at different Ge(IV)/Ge(II) ratios changes the seed concentration (*via* the equilibrium reaction in eq 3), which ultimately leads to different-sized NCs. It is also likely that competing nucleation and growth occurs during reduction of **[Ge(IV)]**. Multiple nucleation events owing to **[Ge(IV)]** reduction (from GeI_4 or produced *via* the equilibrium reaction in eq 3) during the higher-temperature phase would account for the size distribution (*ca.* 20%) observed for all particle sizes.

For the extreme sizes produced using solely GeI_4, the degree of nucleation appears to be controlled by the temperature ramp rate above 250 °C rather than at the lower temperatures in the presence of **[Ge(II)]**. The observations above suggest that a slower ramp rate (~2.5 °C min^{-1}) allows nucleation and growth from **[Ge(IV)]** to occur in parallel. Following initial seed formation starting at 250 °C, the Ge^0 resulting from further **[Ge(IV)]** decomposition must compete between forming additional seeds or growing existing nuclei *via* condensation. Since this slower ramp rate is a more thermodynamically controlled process that would favor large particles (owing to their lower surface energy), **[Ge(IV)]** reduction preferentially adds to existing particles, yielding 11.3 ± 2.4 nm NCs (**Ge-NC(100/0)$_{slow}$**). In contrast, a faster ramp rate (15 °C min^{-1}) rapidly decomposes **[Ge(IV)]** and consumes most of the available germanium, generating a supersaturated solution that precipitates many small Ge^0 seeds. This rapid nucleation is then followed by a limited nucleation and growth stage, owing to the lack of available **[Ge(IV)]**, and yields 2.3 ± 0.4 nm NCs (**Ge-NC(100/0)$_{fast}$**). Finally, we rule out a mechanism based on oriented attachment or fusion of small crystals, which cannot account for the drastically different sizes observed for **Ge-NC(100/0)$_{fast}$** *versus* the **Ge-NC(100/0)$_{slow}$**. If this mechanism were dominant, the 1 h solution annealing at 300 °C would be expected to generate similar particle sizes for both samples.

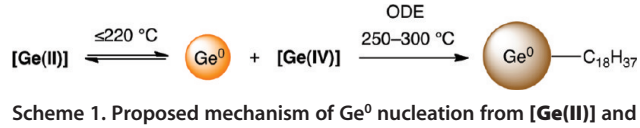

Scheme 1. Proposed mechanism of Ge^0 nucleation from [Ge(II)] and growth from [Ge(IV)]. [Ge(II)] and [Ge(IV)] represent germanium amides or amide−iodide mixed-ligand Ge complexes, as defined in eqs 1 and 2.

In summary, this mixed-valence precursor method is the first solution-phase procedure to provide a high degree of control over both the size and absorption/emission properties of NIR-emitting Ge NCs. The data confirm the two prior reports that quantum-confined Ge bandgap emission is observed in the NIR, not the near-UV to blue-visible. We additionally note that our preliminary investigations have shown that a film of **Ge-NC(0/100)** exhibits solid-state PL emission centered near 900 nm, demonstrating that these NCs hold promise for application in solid-state optoelectronic devices. The mixed-valence reduction synthesis is proposed to occur *via* a mechanism involving Ge^0 seed nucleation from **[Ge(II)]** reduction at moderate temperatures (≤220 °C), and growth from reduction of **[Ge(IV)]** at higher temperatures (250−300 °C). Current research is focused on obtaining greater control over Ge nanoparticle purity, surface passivation, and crystallinity, as well as expanding this synthetic method to other group IV NCs.

METHODS

General. Germanium diiodide (>97%, Gelest GEG5200), germanium tetraiodide (>97%, Gelest GEG5800), and *n*-butyllithium in hexanes (1.6 M, Aldrich) were stored under nitrogen inert atmosphere in a Vacuum Atmospheres glovebox and used as received. 1-Octadecene (ODE, 90%, Aldrich) was distilled under vacuum (5×10^{-3} Torr) from molten sodium prior to storage and use in the glovebox. Hexadecylamine (HDA, 98%, Aldrich) and oleylamine (90%, Aldrich) were degassed and dehydrated under vacuum (5×10^{-3} Torr) at 120 °C prior to storage and use in the glovebox. Common solvents (*i.e.*, toluene, methanol, acetone) used in the nanocrystal purifications were used as received (Aldrich or Fisher, ACS grade) under ambient conditions. Tetrachloroethylene was dried over calcium chloride and distilled under nitrogen prior to storage and use in the glovebox. Hexane was dried through an alumina column prior to use in TEM sample preparation.

Synthesis of Ge-NC(Ge(IV)/Ge(II)) Materials. In a glovebox, a quartz 50-mL three-neck round-bottom flask fitted with a reflux condenser was charged with 3 g of HDA (or oleylamine) and the appropriate amount of GeI_4 and/or GeI_2 to obtain the desired Ge(IV)/Ge(II) ratio. The total Ge content of each reaction was 6.1×10^{-4} mol. The other two inlets of the reaction flask were capped with septa. Also in the glovebox, BuLi (1.1 equiv *vs* total iodide) was diluted with 3 mL of ODE and sealed in a gastight syringe for transfer to the fume hood. The reaction flask was connected to an inert gas-vacuum (Schlenk) manifold and heated under nitrogen flow to 200 at 5 °C min^{-1}. At 200 °C, the BuLi/ODE solution was rapidly injected, and the temperature decreased to *ca.* 150 °C. After 5 min, the temperature had recovered to 200 °C, and was then increased to 300 °C (ramp rate ~2.5 °C min^{-1} for all experiments except for **Ge-NC(100/0)$_{fast}$**, where it was 15 °C min^{-1}) and held for 1 h. The reaction undergoes characteristic color changes from yellow to orange to brown associated with the formation of Ge NCs. After 1 h at 300 °C, the dark brown reaction solution was cooled to 100 °C and transferred to a centrifuge tube with 10 mL of toluene. The nanocrystals were precipitated by adding 25 mL of methanol, and separated by centrifugation (10000 *g*). After decanting the supernatant, the precipitate was resuspended in 10 mL of toluene, and 30 mL of 1:1 (v/v) acetone/methanol was added as nonsolvent. The nanocrystals were again separated by centrifugation. The dissolution−precipitation−centrifugation step was repeated twice using toluene as solvent and 1:1 acetone/methanol as nonsolvent. This procedure yielded 100−150 mg of a brown solid product that was stored in the glovebox.

Characterization. Samples for transmission electron microscopy (TEM) were prepared in a glovebox by drop-casting a solution of Ge nanocrystals in dry hexane onto lacey-carbon-coated copper grids (Ted Pella, part no. 01824). Imaging was performed on an FEI Tecnai T30 electron microscope operating at 300 kV and energy dispersive X-ray spectroscopy (EDS) was recorded *in situ* with an EDAX detector. Average particle diameters and standard deviations were determined by counting >300 particles for each preparation and applying standard statistical analysis. X-ray diffraction (XRD) was performed using a Bruker D8 Discovery system with CCD camera on Ge NC films drop-cast from toluene solutions on a glass slide. Samples of the Ge NCs for absorption and PL emission spectroscopies were prepared as dilute solutions in dry tetrachloroethylene (absorbance ~1.0 at 400 nm with 1.0 cm path length). Absorption spectra were recorded using a Shimadzu UV-3600 spectrophotometer. Absorption onsets in Tauc plots were determined from best fits to the linear region in each plot, from ~0.1 to ~0.01 absorbance units. The absolute PL quantum yield was measured in a LabSphere integrating sphere, with excitation provided either by a Hg−Xe lamp (404.6 nm line) passed through a monochromator and a band-pass filter, or a Ti:sapphire laser (Spectra Physics Tsunami) centered at 750 nm. Optical density at the excitation wavelength was kept between 0.2−0.4. The excitation and emitted light were coupled into a light guide and routed to a monochromator. Depending on the spectral range of interest, either a CCD (400−1000 nm) or a cooled InGaAs photodiode (800−2100 nm) was used for detection. The resulting InGaAs signal was amplified using a lock-in amplifier referenced to a chopper driver, and spectra were collected by scanning the wavelength range using a monochromator. The CCD signal was collected with 0.5 s exposure and 10−30 accumulations. Background and scatter were accounted for by subtracting a spectrum obtained under identical conditions but with only solvent present in the cuvette. Spectra were then corrected for grating, fiber, sphere, and detector efficiencies using a calibrated lamp. For samples with emission that spanned the ranges of the two detectors, the spectra were correlated at 900 nm. Further details of the procedure for determining PL QY were recently reported.[43]

Acknowledgment. The authors thank A.G. Norman (NREL) for HRTEM analysis of Ge NCs described in this research and Jao van de Lagemaat (NREL) for helpful discussions. The authors gratefully acknowledge funding for this work by the Division of Chemical Sciences, Geosciences, and Biosciences in the Office of Basic Energy Sciences of the U.S. Department of Energy under contract no. DE-AC36-08GO28308.

Supporting Information Available: Histograms from TEM size analysis, representative X-ray diffraction pattern, and UV−vis−NIR absorption spectra of Ge NCs are available (Figures S1−S3). This material is available free of charge *via* the Internet at http://pubs.acs.org.

REFERENCES AND NOTES

1. Alivisatos, A. P. Perspectives on the Physical Chemistry of Semiconductor Nanocrystals. *J. Phys. Chem.* **1996**, *100*, 13226–13239.
2. Beard, M. C.; Knutsen, K. P.; Yu, P.; Luther, J. M.; Song, Q.; Metzger, W. K.; Ellingson, R. J.; Nozik, A. J. Multiple Exciton Generation in Colloidal Silicon Nanocrystals. *Nano Lett.* **2007**, *7*, 2506–2512.
3. Efros, A. L.; Rosen, M. The Electronic Structure of Semiconductor Nanocrystals. *Annu. Rev. Mater. Sci.* **2000**, *30*, 475–521.
4. Shieh, J.; Chen, H. L.; Ko, T. S.; Cheng, H. C.; Chu, T. C. Nanoparticle-Assisted Growth of Porous Germanium Thin Films. *Adv. Mater.* **2004**, *16*, 1121–1124.

5. Bostedt, C.; van Buuren, T.; Willey, T. M.; Franco, N.; Terminello, L. J.; Heske, C.; Moller, T. Strong Quantum-Confinement Effects in the Conduction Band of Germanium Nanocrystals. *Appl. Phys. Lett.* **2004**, *84*, 4056–4058.
6. Philipp, H. R.; Taft, E. A. Optical Constants of Germanium in the Region 1−10 eV. *Phys. Rev.* **1959**, *113*, 1002–1005.
7. Murray, C. B.; Kagan, C. R.; Bawendi, M. G. Self-Organization of CdSe Nanocrystallites into 3-Dimensional Quantum-Dot Superlattices. *Science* **1995**, *270*, 1335–1338.
8. Talapin, D. V.; Murray, C. B. PbSe Nanocrystal Solids for n- and p-Channel Thin Film Field-Effect Transistors. *Science* **2005**, *310*, 86–89.
9. Luther, J. M.; Law, M.; Beard, M. C.; Song, Q.; Reese, M. O.; Ellingson, R. J.; Nozik, A. J. Schottky Solar Cells Based on Colloidal Nanocrystal Films. *Nano Lett.* **2008**, *8*, 3488–3492.
10. Law, M.; Luther, J. M.; Song, O.; Hughes, B. K.; Perkins, C. L.; Nozik, A. J. Structural, Optical, and Electrical Properties of PbSe Nanocrystal Solids Treated Thermally or with Simple Amines. *J. Am. Chem. Soc.* **2008**, *130*, 5974–5985.
11. Taylor, B. R.; Kauzlarich, S. M.; Delgado, G. R.; Lee, H. W. H. Solution Synthesis and Characterization of Quantum Confined Ge Nanoparticles. *Chem. Mater.* **1999**, *11*, 2493–2500.
12. Tanke, R. S.; Kauzlarich, S. M.; Patten, T. E.; Pettigrew, K. A.; Murphy, D. L.; Thompson, M. E.; Lee, H. W. H. Synthesis of Germanium Nanoclusters with Irreversibly Attached Functional Groups: Acetals, Alcohols, Esters, and Polymers. *Chem. Mater.* **2003**, *15*, 1682–1689.
13. Wang, W. Z.; Poudel, B.; Huang, J. Y.; Wang, D. Z.; Kunwar, S.; Ren, Z. F. Synthesis of Gram-Scale Germanium Nanocrystals by a Low-Temperature Inverse Micelle Solvothermal Route. *Nanotechnology* **2005**, *16*, 1126–1129.
14. Wang, W. Z.; Huang, J. Y.; Ren, Z. F. Synthesis of Germanium Nanocubes by a Low-Temperature Inverse Micelle Solvothermal Technique. *Langmuir* **2005**, *21*, 751–754.
15. Chiu, H. W.; Kauzlarich, S. M. Investigation of Reaction Conditions for Optimal Germanium Nanoparticle Production by a Simple Reduction Route. *Chem. Mater.* **2006**, *18*, 1023–1028.
16. Hope-Weeks, L. J. Concentration-Dependent Size Control of Germanium Nanocrystals. *Chem. Lett.* **2005**, *34*, 1526–1527.
17. Wilcoxon, J. P.; Provencio, P. P.; Samara, G. A. Synthesis and Optical Properties of Colloidal Germanium Nanocrystals. *Phys. Rev. B* **2001**, *64*, 035417.
18. Chou, N. H.; Oyler, K. D.; Motl, N. E.; Schaak, R. E. Colloidal Synthesis of Germanium Nanocrystals Using Room-Temperature Benchtop Chemistry. *Chem. Mater.* **2009**, *21*, 4105–4107.
19. Prabakar, S.; Shiohara, A.; Hanada, S.; Fujioka, K.; Yamamoto, K.; Tilley, R. D. Size Controlled Synthesis of Germanium Nanocrystals by Hydride Reducing Agents and Their Biological Applications. *Chem. Mater.* **2010**, *22*, 482–486.
20. Lu, X. M.; Korgel, B. A.; Johnston, K. P. Synthesis of Germanium Nanocrystals in High Temperature Supercritical CO_2. *Nanotechnology* **2005**, *16*, S389–S394.
21. Gerung, H.; Bunge, S. D.; Boyle, T. J.; Brinker, C. J.; Han, S. M. Anhydrous Solution Synthesis of Germanium Nanocrystals from the Germanium(II) Precursor $Ge[N(SiMe_3)_2]_2$. *Chem. Commun.* **2005**, 1914–1916.
22. Gerung, H.; Zhao, Y.; Wang, L.; Jain, R. K.; Boyle, T. J.; Brinker, C. J.; Han, S. M. Two-Photon Absorption of Matrix-free Ge Nanocrystals. *Appl. Phys. Lett.* **2006**, *89*, 111107.
23. Lu, X. M.; Korgel, B. A.; Johnston, K. P. High Yield of Germanium Nanocrystals Synthesized from Germanium Diiodide in Solution. *Chem. Mater.* **2005**, *17*, 6479–6485.
24. Lee, D. C.; Pietryga, J. M.; Robel, I.; Werder, D. J.; Schaller, R. D.; Klimov, V. I. Colloidal Synthesis of Infrared-Emitting Germanium Nanocrystals. *J. Am. Chem. Soc.* **2009**, *131*, 3436–3437.
25. Hayashi, R.; Yamamoto, M.; Tsunetomo, K.; Kohno, K.; Osaka, Y.; Nasu, H. Preparation and Properties of Ge Microcrystals Embedded in SiO_2 Glass-Films. *Jpn. J. Appl. Phys.* **1990**, *29*, 756–759.
26. Maeda, Y.; Tsukamoto, N.; Yazawa, Y.; Kanemitsu, Y.; Masumoto, Y. Visible Photoluminescence of Ge Microcrystals Embedded in SiO_2 Glassy Matrices. *Appl. Phys. Lett.* **1991**, *59*, 3168–3170.
27. Kanemitsu, Y.; Uto, H.; Masumoto, Y.; Maeda, Y. On the Origin of Visible Photoluminescence in Nanometer-Size Ge Crystallites. *Appl. Phys. Lett.* **1992**, *61*, 2187–2189.
28. Maeda, Y. Visible Photoluminescence from Nanocrystallite Ge Embedded in a Glassy SiO_2 Matrix —Evidence in Support of the Quantum-Confinement Mechanism. *Phys. Rev. B* **1995**, *51*, 1658–1670.
29. Craciun, V.; Boulmer-Leborgne, C.; Nicholls, E. J.; Boyd, I. W. Light Emission from Germanium Nanoparticles Formed by Ultraviolet-Assisted Oxidation of Silicon−Germanium. *Appl. Phys. Lett.* **1996**, *69*, 1506–1508.
30. Dutta, A. K. Visible Photoluminescence from Ge Nanocrystal Embedded into a SiO_2 Matrix Fabricated by Atmospheric Pressure Chemical Vapor Deposition. *Appl. Phys. Lett.* **1996**, *68*, 1189–1191.
31. Min, K. S.; Shcheglov, K. V.; Yang, C. M.; Atwater, H. A.; Brongersma, M. L.; Polman, A. The Role of Quantum-Confined Excitons *versus* Defects in the Visible Luminescence of SiO_2 Films Containing Ge Nanocrystals. *Appl. Phys. Lett.* **1996**, *68*, 2511–2513.
32. Zacharias, M.; Fauchet, P. M. Blue Luminescence in Films Containing Ge and GeO_2 Nanocrystals: The Role of Defects. *Appl. Phys. Lett.* **1997**, *71*, 380–382.
33. Takeoka, S.; Fujii, M.; Hayashi, S.; Yamamoto, K. Size-Dependent Near-Infrared Photoluminescence from Ge Nanocrystals Embedded in SiO_2 Matrices. *Phys. Rev. B* **1998**, *58*, 7921–7925.
34. Nakamura, Y.; Watanabe, K.; Fukuzawa, Y.; Ichikawa, M. Observation of the Quantum-Confinement Effect in Individual Ge Nanocrystals on Oxidized Si Substrates Using Scanning Tunneling Spectroscopy. *Appl. Phys. Lett.* **2005**, *87*, 133119.
35. Bostedt, C.; van Buuren, T.; Plitzko, J. M.; Moller, T.; Terminello, L. J. Evidence for Cubic Phase in Deposited Germanium Nanocrystals. *J. Phys.: Condens. Matter* **2003**, *15*, 1017–1028.
36. Gresback, R.; Holman, Z.; Kortshagen, U. Nonthermal Plasma Synthesis of Size-Controlled, Monodisperse, Freestanding Germanium Nanocrystals. *Appl. Phys. Lett.* **2007**, *91*, 093119.
37. Reboredo, F. A.; Zunger, A. L-to-X Crossover in the Conduction-Band Minimum of Ge Quantum Dots. *Phys. Rev. B* **2000**, *62*, R2275–R2278.
38. Niquet, Y. M.; Allan, G.; Delerue, C.; Lannoo, M. Quantum Confinement in Germanium Nanocyrstals. *Appl. Phys. Lett.* **2000**, *77*, 1182–1184.
39. Haynes, J. R. New Radiation Resulting from Recombination of Holes and Electrons in Germanium. *Phys. Rev.* **1955**, *98*, 1866–1868.
40. While the present manuscript was under revisions, a publication appeared (Vaughn II, D. D.; Bondi, J. F.; Schaak, R. E. Colloidal Synthesis of Air-Stable Crystalline Germanium Nanoparticles with Tunable Sizes and Shapes. *Chem Mater.* **2010**, *22*, 6103−6108) detailing a method for preparing non-emitting 6−22 nm Ge NCs. Although the UV−vis absorption spectra showed some variation with particle size, it is difficult to evaluate the bandgap of these NCs as no Tauc plots were performed.
41. Buriak, J. M. Organometallic Chemistry on Silicon and Germanium Surfaces. *Chem. Rev.* **2002**, *102*, 1271–1308.
42. Kortshagen, U. Nonthermal Plasma Synthesis of Semiconductor Nanocrystals. *J. Phys. D* **2009**, *42*, 113001.
43. Semonin, O. E.; Johnson, J. C.; Luther, J. M.; Midgett, A. G.; Nozik, A. J.; Beard, M. C. Absolute Photoluminescence Quantum Yields of IR-26 Dye, PbS, and PbSe Quantum Dots. *J. Phys. Chem. Lett.* **2010**, *1*, 2445–2450.

44. Sykora, M.; Koposov, A. Y.; McGuire, J. A.; Schulze, R. K.; Tretiak, O.; Pietryga, J. M.; Klimov, V. I. Effect of Air Exposure on Surface Properties, Electronic Structure, and Carrier Relaxation in PbSe Nanocrystals. *ACS Nano* **2010**, *4*, 2021–2034.
45. Armatas, G. S.; Kanatzidis, M. G. Size Dependence in Hexagonal Mesoporous Germanium: Pore Wall Thickness *versus* Energy Gap and Photoluminescence. *Nano Lett.* **2010**, *10*, 3330–3336.
46. Johnson, W. C.; Sidwell, A. E. Nitrogen Compounds of Germanium. IV. The Action of Ammonia and Amines on Germanium Tetraiodide. *J. Am. Chem. Soc.* **1933**, *55*, 1884–1889.
47. Eisenhuth, W.; Van Wazer, J. R. *N*-Methylated Perchlorogermazanes and the Reaction of Germanium Tetrachloride with Methylamine. *Inorg. Chem.* **1968**, *7*, 1642–1645.
48. Henderson, E. J.; Veinot, J. G. C. Synthesis of Oxide Encapsulated and Freestanding Hydride Surface Terminated $Si_{1-x}Ge_x$ Nanocrystals. *Chem. Mater.* **2007**, *19*, 1886–1888.